Transaction A: Civil Engineering
Vol. 16, No. 3, pp. 189–198

SCIENTIA IRANICA

Implementation and Comparison of a Generalized Plasticity and Disturbed State Concept for the Load-Deformation Behavior of Foundations

A.H. Akhaveissy[1,*], C.S. Desai[2], S.A. Sadrnejad[3] and H. Shakib[4]

Abstract. *A nonlinear finite element method with an eight-noded isoparametric quadrilateral element is used for the prediction of load-deformation behavior including the bearing capacity of foundations. A Disturbed State Concept (DSC) with a Hierarchical Single-Surface (HISS) plasticity model with an associated flow rule, and a Generalized Plasticity Model (GPM) with a non-associated flow rule are used to characterize the constitutive behavior of soils. The DSC model, however, can allow for non-associative behavior through the use of disturbance. Both models are able to simulate load-deformation including softening behavior. However, the GPM is based on the continuum approach while the DSC can allow for discontinuity due to factors such as microcracking. Predictions by both models show good agreement with laboratory data. A comparison between the DSC/HISS and generalized plasticity model is presented and it is found that the DSC/HISS model has certain advantages over the generalized plasticity model. A modified Terzaghi theory is developed for the bearing capacity based on the dependence of material behavior and in-situ stress; it can be used to compute the bearing capacity affected by in-situ stress.*

Keywords: *Generalized plasticity; Hiss plasticity; Non-associated flow rule; Terzaghi theory.*

INTRODUCTION

The main objective is to implement two available models in a finite element procedure for load-deformation behavior for geotechnical problems. The parameters for both models for sand are derived from laboratory triaxial stress-strain curves under various confining pressures. Then, the models are validated at the element level by comparison of the prediction with laboratory data. For practical problems, the models are validated with respect to the load-deformation behavior of footing on sand.

Constitutive models to analyze geotechnical problems by the finite element method are usually based on von Mises and Drucker-Prager criterion (e.g. [1-5]). Although Drucker-Prager and von Mises models are commonly used, they may not provide sufficient generality in terms of stress path dependency and coupling of the volumetric and shear responses. Desai et al. in [3] analyzed a footing on artificial material by use of the Drucker-Prager, critical state and modified cap model. They found that the modified cap model provided better results. Faruque and Desai [6] analyzed a footing as three dimensional by using a generalized constitutive model. Altaee et al. [7] analyzed footing on artificial material by use of a bounding surface model. They compared their results of the bounding surface plasticity model with those of the Drucker-Prager, critical state and modified cap model, and showed that the bounding surface results were better than those from the other models. Lee and Salgado [8] estimated the bearing capacity of circular footings on sands based on the cone penetration test. They used the elastic shear modulus in the analysis as a function of the second invariant of deviatoric stress in order to obtain load-deformation curves. In order to describe failure and post-failure soil response, the Drucker-Prager failure criterion was adopted by Lee and Salgado. They obtained load-settlement curves from finite element analyses for different footing sizes

1. *Department of Civil Engineering, Razi University, Kermanshah, P.O. Box 67149-67346, Iran.*
2. *Department of Civil Engineering and Engineering Mechanics, University of Arizona, Tucson, AZ, P.O. Box 85721, USA.*
3. *Department of Civil Engineering, Khajeh-Nasir Toosi University of Technology, Tehran, P.O. Box 19967-15433, Iran.*
4. *Department of Civil Engineering, Tarbiat Modares University, Tehran, P.O. Box 14115-143, Iran.*
*. *Corresponding author. E-mail: AHAKHAVEISSY@razi.ac.ir*

Received 2 July 2007; received in revised form 8 September 2007; accepted 5 April 2008

and relative densities ($D_r = 30$, 50, 70 and 90%). The predicted load-settlement curves did not show a limit load. Therefore, they adopted the load at a settlement equal to 20% of the footing diameter as the limiting bearing capacity of the footing. It was found that both the relative density, D_r, and the lateral earth pressure ratio, K_0, are important factors affecting load-deformation curves; the effect of K_0 being greater for lower D_r values. The allowable load at a 25 mm settlement was also studied.

In this paper, the GP (Generalized Plasticity) and the DSC/HISS (disturbed state concept/hierarchical single-surface) plasticity model are implemented to analyze a footing on sand. These models are able to simulate softening behavior and provide predictions of the load-deformation behavior of footings, which are compared with laboratory data. The DSC/HISS model possesses certain advantages over the generalized plasticity model. Then, based on predicted load-deformation curves, a formula is proposed to determine the bearing capacity of footing as affected by in-situ stress.

FORMULATION

For analysis of a soil-footing system, a generalized plasticity theory and disturbed state concept are applied by using the finite element program in SSINA2D [9] (Soil Structure Interaction Nonlinear Analysis, two Dimensional). Descriptions of the two models are given below.

Generalized Plasticity Model

Zienkiewicz et al. [10] applied a bounding surface theory as the generalized plasticity model for analysis of the static and transient loading on soils. They used the critical state yield surface and modified plastic modulus, and defined a plastic modulus as being the product of a function of the derivative of the yield surface with respect to plastic strain and a nonlinear function of distance between the current yield surface and the bounding surface. The method of analysis for sand is described in [11]. Chen and Baladi [12] expressed stress-strain relations in terms of the hydrostatic and deviatoric components of strain and stress; this relation can be used simply if there are plasticity moduli and components of the flow rule vector in terms of the hydrostatic and deviatoric components of stress. Pastor et al. [13] proposed a plastic modulus and flow rule dependent on the dilatancy of soil without using special yield and potential surfaces [13]. They defined components of the flow rule in the directions of volumetric and shear deformations. Therefore, the analysis of geotechnical problems can be implemented by expressed relations in [12,13]. Liu et al. [14,15] proposed some changes in the plastic modulus for analysis of cyclic loading on soils.

In the present work, the relations are reformulated as general, and the unit vector normal to yield and the potential surface are determined from the yield and potential surface, while Pastor et al. [13] defined flow rule as a function of dilatancy without using the yield and potential surface. The flow rule was defined in the direction of the volumetric (n_v) and shear strain (n_s) as [13]:

$$n = (n_v, n_s), \tag{1a}$$

$$n_v = \frac{d}{\sqrt{(1+d^2)}}, \tag{1b}$$

$$n_s = \frac{1}{\sqrt{(1+d^2)}}, \tag{1c}$$

where d represents the dilation in soil and is expressed as:

$$d = \frac{d\varepsilon_v^p}{d\varepsilon_s^p} = (1+\alpha)(M-\eta), \tag{2a}$$

$$\eta = \frac{q}{p}, \tag{2b}$$

where M can be used as M_g and M_f, which are as the slopes defining zero dilatancy (Figure 1) and α is the material parameter. The yield (f) and potential surfaces (g) are found using Equations 1 and 2 as [13]:

$$f = q - M_f \times p \times (1 + 1/\alpha) \times \left(1 - \left(\frac{p}{p_e}\right)^{\alpha}\right), \tag{3a}$$

$$g = q - M_g \times p \times (1 + 1/\alpha) \times \left(1 - \left(\frac{p}{p_g}\right)^{\alpha}\right). \tag{3b}$$

These surfaces are shown schematically in Figure 1, where $p = I_1$ and $q = \sqrt{3J_{2D}}$. p_e and p_g are the mean of initial normal stresses and I_1 and J_{2D} are the first

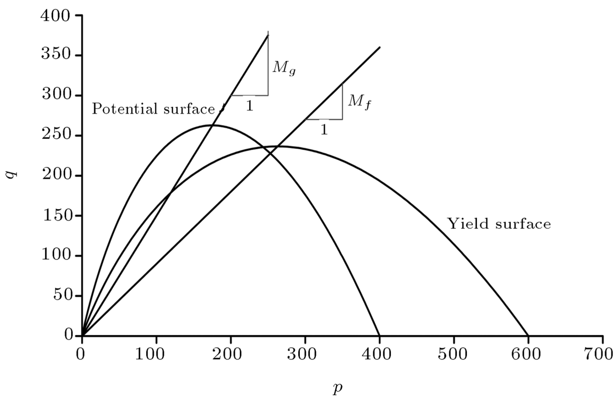

Figure 1. Schematic yield and potential surfaces.

invariant of the stress tensor and the second invariant of the deviatoric stress tensor, respectively.

The unit vectors normal to yield (f) and potential surface (g) can be defined as:

$$n = \frac{\frac{\partial f}{\partial \sigma}}{\left[\frac{\partial f}{\partial \sigma} : \frac{\partial f}{\partial \sigma}\right]^{\frac{1}{2}}}, \tag{4a}$$

$$n_g = \frac{\frac{\partial g}{\partial \sigma}}{\left[\frac{\partial g}{\partial \sigma} : \frac{\partial g}{\partial \sigma}\right]^{\frac{1}{2}}}. \tag{4b}$$

The derivatives in Equation 4 can be written as:

$$\frac{\partial f}{\partial \sigma} = C_1 \frac{\partial I_1}{\partial \sigma} + C_2 \frac{\partial \sqrt{J_{2D}}}{\partial \sigma} + C_3 \frac{\partial J_{3D}}{\partial \sigma}, \tag{5}$$

where J_{3D} is the third invariant of the deviatoric stress tensor. M_f and M_g depend on the Lode angle [13] but, here, they are assumed as a constant; therefore, the derivative of the yield surface with respect to J_{3D}, C_3, is zero. C_1 and C_2 are as follows:

$$C_1 = \frac{\partial f}{\partial I_1} = (1+\alpha)\left(\frac{M_f}{3} - \frac{\sqrt{3 J_{2D}}}{I_1}\right), \tag{6a}$$

$$C_2 = \sqrt{3}. \tag{6b}$$

If M_g is substituted instead of M_f, coefficient C_1 relates to the potential surface. The increment of stress can be determined in the finite element method as follows [13]:

$$d\sigma = \left(C_e - \frac{C_e n_g . n^T C_e}{H + n^T C_e n_g}\right) d\varepsilon, \tag{7}$$

where H is the plastic modulus [13]. The plastic modulus for the loading case requires 6 parameters: Initial plastic modulus (H_0); slope of phase change line (M_f, M_g); three parameters that define the plastic strain expansive (α, β_0, β_1) and two parameters for the unloading case (H_{u0}, γ_u). Also, two parameters define the elastic strain increment (E, υ). Therefore, the increment of stress can be found by using Equations 4 to 7. It must be noted that the sign of the volumetric component of the vector perpendicular on the potential surface was altered in [13] as a constraint, but in the present work, in accordance to Equations 5 and 6, the sign of the vector is not changed.

Disturbed State Concept with HISS Model

In the DSC model, a deforming material element is assumed to be composed of two reference states: The Relatively Intact (RI), and the Fully Adjusted (FA) (Figure 2). The observed behavior is expressed in terms of that of RI and FA states, using the disturbance

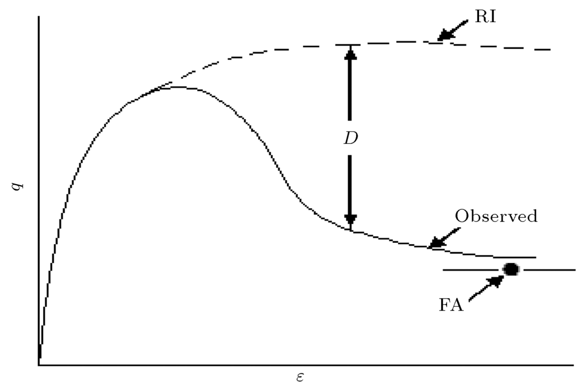

Figure 2. Disturbance as coupling between RI and FA states [16].

function, D, which acts as a coupling or interaction mechanism between RI and FA states (Figure 2). Disturbance grows as the material deforms and the plastic strain increases. Thus, DSC is the only model that includes the coupling intrinsically in which the micro cracked or fully adjusted part also contributes to the response of the material. The RI and FA states can be defined by using various models. The continuum elasticity or plasticity can be used for modeling the response of the RI state while the FA state can be assumed to carry only hydrostatic stress, or it can be modeled by using the critical state model [16]. Following is a brief description of the models for the RI and FA states used in this research.

Relative Intact (RI) and Fully Adjusted (FA) States

The Hierarchical Single-Surface (HISS) plasticity models provide a general formulation for the elastoplastic characterization of the material behavior. These models, which can allow for isotropic and anisotropic hardening and associated and nonassociated plasticity characterizations, can be used to represent the material response, based on the continuum plasticity theory [16]. Usually, the RI state is defined by the associated plasticity model in a Hierarchical Single-Surface (HISS) approach. The yield function, F, is given by [16]:

$$F = \overline{J}_{2D} - (-\alpha \overline{J}_1^n + \gamma \overline{J}_1^2)(1 - \beta S_r)^{-0.5} = 0, \tag{8a}$$

$$\overline{J}_{2D} = \frac{J_{2D}}{p_a^2}, \tag{8b}$$

$$\overline{J}_1 = (J_1 + 3R)/p_a, \tag{8c}$$

$$S_r = \frac{\sqrt{27}}{2} . \frac{J_{3D}}{J_{2D}^{1.5}}, \tag{8d}$$

where J_{3D} and J_{2D} are the third and second invariant of deviatoric stress; J_1 is the first invariant of stress; p_a is the atmospheric pressure and R is the bonding stress used mainly to include the cohesive strength ($\bar{c}$) (Figure 3). γ and β parameters are related to the ultimate condition and the hardening or growth function can be expressed as:

$$\alpha = \frac{a_1}{\xi^{\eta_1}}, \tag{9}$$

where a_1 and η_1 are material parameters and ξ is the trajectory of plastic strains. Using F, Equation 8a, the stress-strain equations are derived as [16]:

$$d\sigma = \left[C^e - \frac{C^e \left(\frac{\partial Q}{\partial \sigma}\right)\left(\frac{\partial F}{\partial \sigma}\right)^T C^e}{\left(\frac{\partial F}{\partial \sigma}\right)^T C^e \left(\frac{\partial Q}{\partial \sigma}\right) - \frac{\partial F}{\partial \xi}\gamma_F} \right] d\varepsilon, \tag{10a}$$

$$\gamma_F = \left[\left(\frac{\partial Q}{\partial \sigma}\right)^T \left(\frac{\partial Q}{\partial \sigma}\right) \right]^{1/2}. \tag{10b}$$

C^e is the elastic constitutive matrix and here it is adopted as the associated flow rule ($F = Q$). By the use of Equation 10, the increment of stress for RI is found.

The FA state can be modeled by using the critical state model [16,17]. The material is assumed to shear under a constant volume or a constant void ratio.

Disturbance (D)

Disturbance, D, for the interaction between relatively intact and fully adjusted parts can be defined in terms of the plastic strain as:

$$D = D_u[1 - \exp(-A\xi_D^Z)], \tag{11}$$

where D_u is the ultimate disturbance (often assumed to be unity), ξ_D is the trajectory of deviatoric plastic strains, and A and Z are disturbance parameters.

The RI and FA states both contribute to the material response with disturbance (D) as the coupling function. Following DSC equations in the incremental form, this coupling is shown mathematically [16].

$$d\sigma_{ij}^a = (1 - D)d\sigma_{ij}^i + Dd\sigma_{ij}^c + dD(d\sigma_{ij}^c - d\sigma_{ij}^i), \tag{12}$$

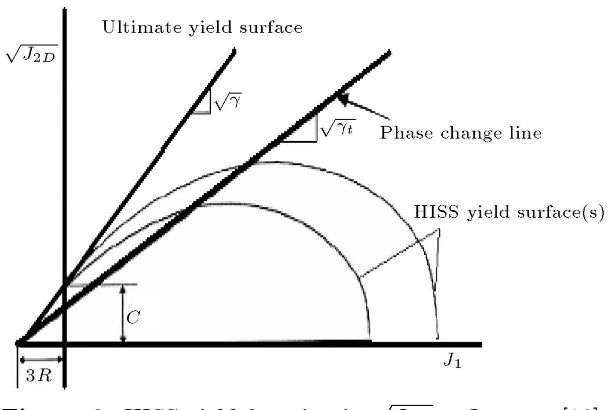

Figure 3. HISS yield function in $\sqrt{J_{2D}} - J_1$ space [16].

where d denotes the increment or rate, σ_{ij} is the stress tensor and the superscripts i, a, and c represent RI, observed and FA states, respectively.

Comparison of DSC/HISS and Generalized Plasticity Model

The DSC/HISS and generalized plasticity models are able to simulate hardening and softening behavior. The generalized plasticity model is able to simulate liquefaction and cyclic mobility phenomena for undrained sand [13]. DSC/HISS is applicable to many materials including soils, rocks, concrete, alloys and silicon [16]. The DSC/HISS model allows for discontinuities induced during deformation. However, most plasticity models, including GPM, are based on a continuum approach. Hence, the DSC/HISS model is considered to be an improvement over GPM when softening as degradation occurs.

NUMERICAL SIMULATION OF LOAD-DEFORMATION OF FOUNDATION

Laboratory Material Test

Artificial soil [7], Tehran sand [18] and Houston sand are used for the analysis of a footing system, but only the results of artificial soil and Tehran sand [18] are considered herein. Figures 4a and 4b show laboratory triaxial stress-strain curves under various confining pressures, σ_3, for artificial soil and Tehran sand, respectively. The parameters of both DSC/HISS and GPM are determined for triaxial stress-strain curves, as shown in Figure 4.

Determination of Parameters

A brief explanation to determine HISS model parameters follows:

1. Ultimate parameters, γ and β. The parameter, γ, represents the asymptotic ultimate stress. The yield surface becomes, approximately, a straight line in the $J_1 - \sqrt{J_{2D}}$ space when the hardening parameter, α, is zero. The parameter, β, controls the shape yield surface in the octahedral plane. Three compression tests are used to determine the value of parameters γ and β. The corresponding asymptotic values of J_1 and $\sqrt{J_{2D}}$ for all the three tests are used to calculate the ultimate parameters, γ and β, by a least square procedure program. The parameters for Tehran sand are determined in Figure 5. β can be found in Equation 8a when α is zero.
2. Phase change parameter n. The value of n can be found from the slopes of the phase change line, γ_t,

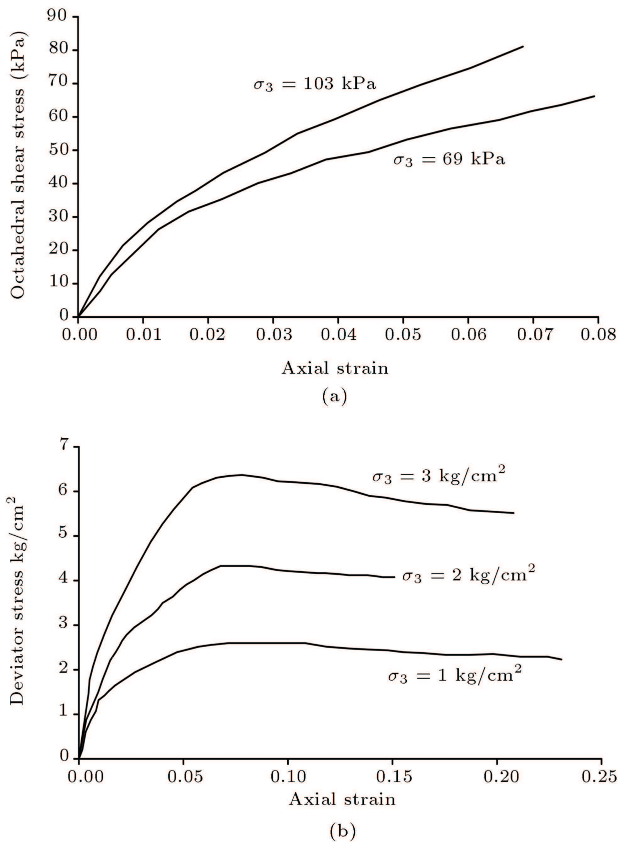

Figure 4. Laboratories triaxial test data for (a) Artificial soil [7] and (b) Tehran sand [18].

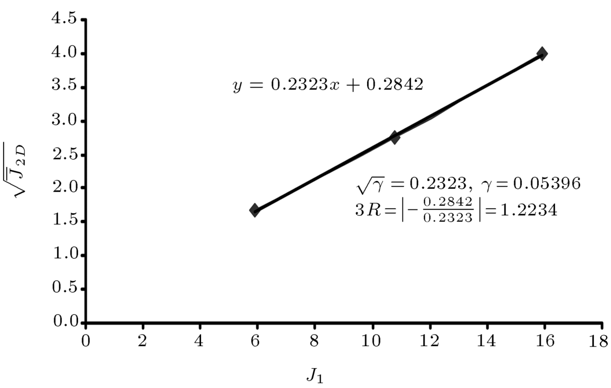

Figure 5. Asymptotic state for Tehran sand.

and the ultimate line, γ, [16], as follows:

$$\frac{\gamma_t}{\gamma} = \left(\frac{n-2}{n}\right)^{0.5}. \tag{13}$$

3. Hardening parameters, a_1 and η_1. The proposed hardening function, α, is expressed in terms of the plastic strain trajectory, or the accumulated plastic strain. Taking the natural logarithm on both sides of Equation 9 leads to:

$$\ln(\alpha) = \ln(a_1) - \eta_1 \ln(\xi). \tag{14}$$

From each compression test, the values of α are calculated for several stress points, using the yield function, $F = 0$. Knowing α and ξ, one can determine the best fit line for the set of points $[\ln(\alpha), \ln(\xi)]$, in order to evaluate the values of parameters a_1 and η_1. For example, Figure 6 shows the $\ln(\alpha)$ vs. $\ln(\xi)$ plot for the compression test of Tehran sand with confining pressure 1 kg/cm^2.

In this study, the parameters for generalized plasticity and DSC/HISS plasticity models are determined, based on conventional triaxial compression tests (Figure 7 and Tables 1 and 2). Ultimate disturbance, $D_u = 1$, and atmospheric pressure, $p_a = 101.3$ kPa, are adopted.

Validations

The models are validated at the element level by using the parameters in Tables 1 and 2 and Equations 7 and 12. Figure 7 shows a comparison between the predictions from the models and the laboratories data for the two sands.

It is clear in Figure 7 that the results from both models are in good agreement with laboratory data.

Applications

Numerical simulations of footing load response and bearing capacity are considered for different sands, based on parameters given in Tables 1 and 2. In the first step, analyses of footing on artificial soil are obtained and the results are compared with observed data in the laboratory. In the next step, load-displacement behavior and bearing capacity are determined for a footing on Tehran and Houston sands for different in-situ stresses using DSC/HISS and GPM models. Then, the results are also compared with those using PLAXIS 7.2 [9], which is a program to analyze geotechnical problems. Based on these results, an expression is derived to determine the bearing capacity of footings.

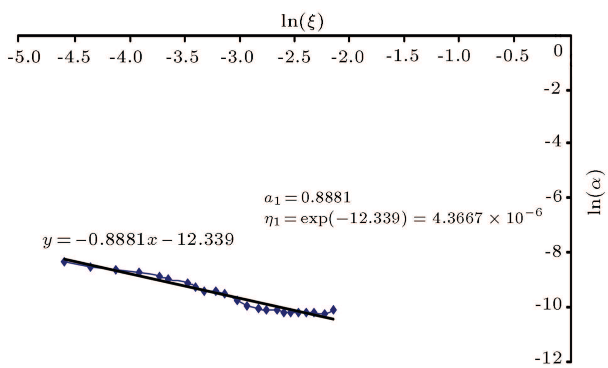

Figure 6. Determination of parameters a_1 and η_1 for Tehran sand.

Table 1. Parameters for Generalized Plasticity Model (GPM).

Kind of Sand	Confining Pressure	E	v	M_f	M_g	$H0$	β_0	β_1	α	$Hu0$	γ_u
Artificial	69 (kPa)	15000 (kPa)	0.35	1.0	1.38	125	0.5	0.2	0.4	2000	0.005
	103 (kPa)	15000 (kPa)	0.35	1.0	1.38	125	0.5	0.2	0.6	2000	0.005
Houston	350 (kPa)	229000 (kPa)	0.37	0.8	0.88	2800	2.55	0.4	0.57	125000	0.005
Tehran	1 (kg/cm^2)	850 (kg/cm^2)	0.35	0.75	0.86	270	0.8	0.85	0.34	100	0.1
	2 & 3 (kg/cm^2)	850 (kg/cm^2)	0.35	0.7	0.95	80	3.6	0.12	0.13	100	0.1

Table 2. Parameters for DSC model.

Kind of Sand	Confining Pressure	HISS Parameters									DSC Parameters
	σ_3	E	v	γ	β	n	R	a_1	η_1	A	Z
Artificial	69 (kPa)	15000 (kPa)	0.35	0.0950	0.000	5.200	0.000	2.4e-4	0.8371	-	-
	103 (kPa)	15000 (kPa)	0.35	0.0950	0.000	5.200	0.000	4.0e-5	0.8371	-	-
Houston Sand	203 (kPa)	229000 (kPa)	0.37	0.0838	1.34e-3	6.97	31.53	1e-9	0.8371	-	-
	350 (kPa)	229000 (kPa)	0.37	0.0838	1.34e-3	6.97	31.53	1.35e-10	0.8371	-	-
	500 (kPa)	229000 (kPa)	0.37	0.0838	2.31e-5	6.97	31.53	2e-11	0.8371	-	-
Tehran	1 (kg/cm^2)	850 (kg/cm^2)	0.35	0.0539	0.042	4.759	0.408	4.37E-6	0.8881	1317.1	3.67
	2 (kg/cm^2)	850 (kg/cm^2)	0.35	0.0539	0.0162	4.759	0.408	8.00E-7	1.0314	579.6	3.19
	3 (kg/cm^2)	850 (kg/cm^2)	0.35	0.0539	0.0162	4.759	0.408	2.40e-7	1.0314	579. 6	3.19

Footing on Artificial Sand

The finite element program is used to analyze the behavior of a model-scale footing; the details of the model-scale footing test were reported in [7]. A rigid rectangular box of size 114 × 203 × 876 mm is used as a container. The footing is 76 mm wide, 19 mm thick and 114 mm long, as shown in Figure 8, and is placed at the center of the box. A vertical load is applied on the footing in increments at the center of the footing. Measurements are taken for vertical displacements corresponding to each load increment.

Initial in-situ vertical stresses in the soil mass are calculated on the basis of the soil density (2000 kg/m^3). Horizontal stresses are taken equal to vertical stress ($K_0 = 1$), as reported in [7], where K_0 is the coefficient of earth pressure at rest. The model scale footing is analyzed with the plain strain idealization. Because of the symmetry, only one half of the soil-footing system is considered. Figure 9 shows the finite element mesh used in the analysis, it consists of 253 eight-noded isoparametric quadrilateral elements, whereas 120 elements were used in [7].

The observed load-displacement relation of the model-scale footing from laboratory data and the results of the finite element analysis in the present study are compared in Figure 10, which also includes the results of reported finite element analyses in [7], together with results obtained by using critical state, bounding surface, Drucker-Prager and modified cap models. Comparisons show that the generalized plasticity and HISS (here, only the HISS plasticity model is used) models are able to simulate the behavior of the footing-soil system. As illustrated in Figure 10, the best result is obtained from generalized plasticity and HISS plasticity models. Also, Drucker-Prager gives a small settlement before the limit load, because it behaves as elastic prior to the limit load and the critical state shows a stiffer behavior than that of the modified cap model. The critical state model is based on a mathematical relation, while the modified cap model has been obtained from many test data in laboratories. Therefore, the modified cap model provides better results than the critical state model. Also, the hardening rule, in both the critical state and modified cap model, is defined as a function of the plastic volumetric strain,

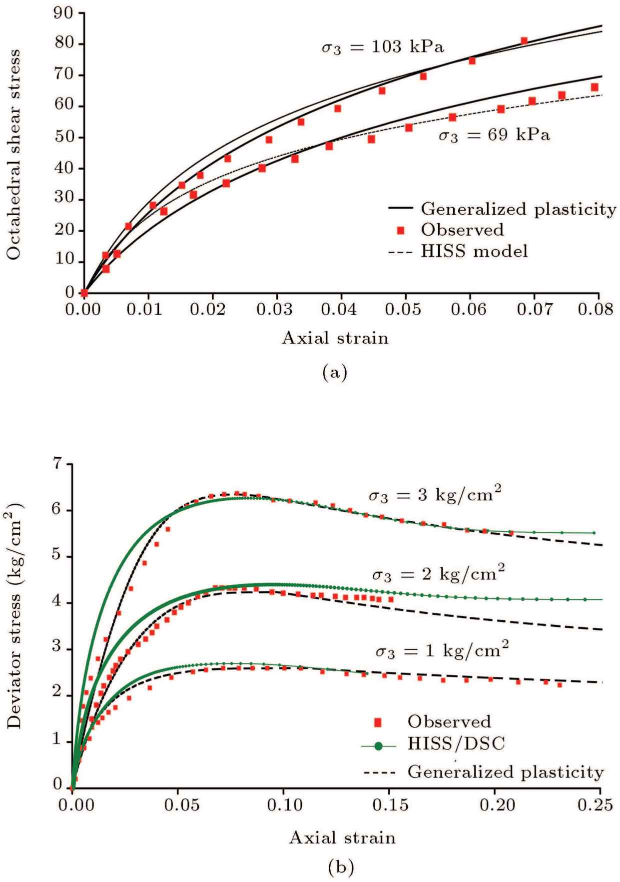

Figure 7. Comparison predictions and laboratory data for (a) Artificial soil and (b) Tehran sand.

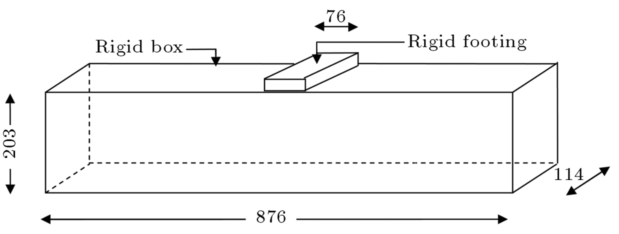

Figure 8. Layout of model-scale footing [7] (dimension is in mm).

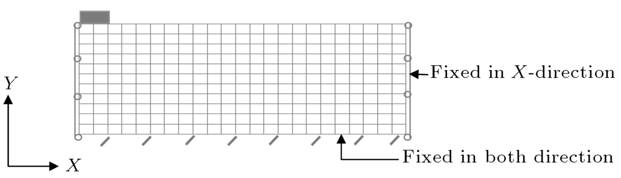

Figure 9. Finite element mesh for the footing.

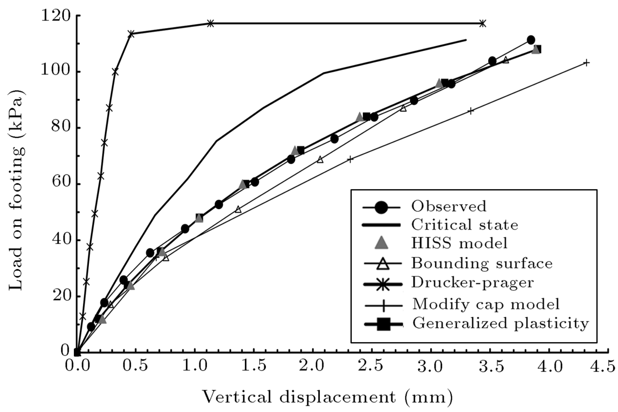

Figure 10. Comparison of load-displacement curves for different models.

whereas the HISS and generalized plasticity model is defined as a function of the plastic volumetric and plastic shear strain. In accordance with failure surfaces in soil below a foundation, shear deformation is more effective than volumetric deformation in determination of the ultimate load and load-displacement behavior of the footing system. Also, the yield surface of the HISS and generalized plasticity model grows with continuous hardening and, finally, approaches ultimate yield. Therefore, predictions by both generalized plasticity and HISS models show good agreement with laboratory data.

Footing on Tehran Sand

The finite element procedure is used to analyze a strip square footing of 200 cm width on Tehran sand for different in-situ stress. It is assumed that the in-situ stress is constant with depth. Figure 11 shows the boundary condition of the problem; 200 eight-noded isoparametric quadrilateral elements are used to model the soil. A soil density of 1.73 gr/cm^3 and a friction angle of 31 degrees were reported in [18]. For Tehran sand, analyses are obtained for both generalized plasticity and DSC/HISS models by using the parameters in Tables 1 and 2 for Tehran sand.

Figures 12 and 13 show the results of finite element analyses for in-situ stress equal to 1.0 and 3.0 kg/cm^2, respectively. This problem also is analyzed by PLAXIS 7.2 [9] for friction angle of 31° and both in-situ stresses. The Mohr-Coulomb criterion is used to analyze the footing by PLAXIS. Predictions by

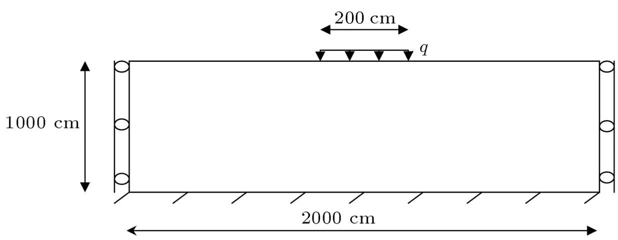

Figure 11. Boundary condition of footing-soil system.

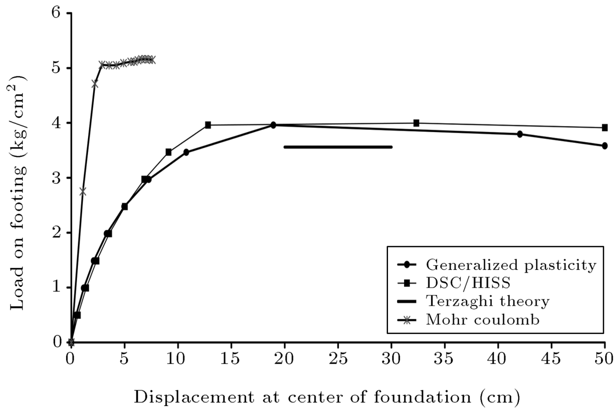

Figure 12. Load-displacement curve for in-situ stress equal to 1.0 kg/cm^2.

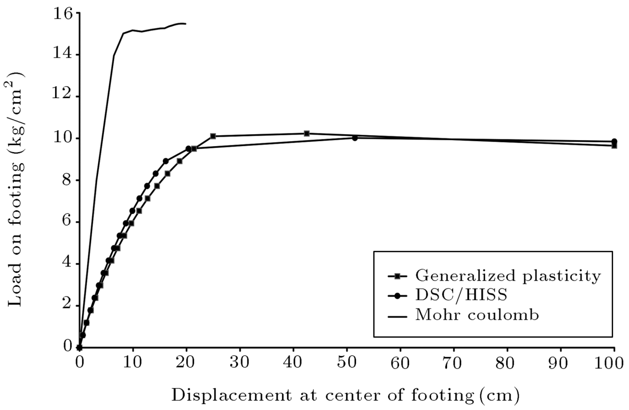

Figure 13. Load-displacement curve for in-situ stress equal to 3.0 kg/cm^2.

GPM, DSC/HISS and Mohr-Coulomb are compared in Figures 12 and 13.

GPM and DSC/HISS models are able to simulate the softening behavior of sand for dense sand. Both models (Figures 12 and 13) show that the bearing capacity is essentially the same. Due to elastic-perfectly plastic behavior, Mohr-Coulomb and Drucker-Prager give less deformation prior to ultimate load than other models. In other words, there is no plastic deformation prior to the limit load (Figures 10, 12 and 13). The bearing capacity predicted by the Mohr-Coulomb model is greater than that predicted by DSC/HISS and GP models. Also, the Mohr-Coulomb model does not accurately account for the change in bearing capacity with in-situ stress. For example, as shown in Figures 12 and 13, a change in the in-situ stress from 1 kg/cm^2 to 3 kg/cm^2 shows an increase in the predicted bearing capacity. The Mohr-Coulomb model predicts the bearing capacity to be increased from 5.0 kg/cm^2 to 15.0 kg/cm^2 when the in-situ stress changes from 1.0 kg/cm^2 to 3.0 kg/cm^2. However, DSC/HISS and GP models predict an increase from 4 kg/cm^2 to 10 kg/cm^2 for the same increase in the in-situ stress. This subject shows the effect of softening and plastic deformation on the limit load. According to these results, load-displacement curves for Tehran sand are compared in Figure 14 for different in-situ stresses, which were assumed constant with depth.

In considering Figure 14, it is clear that plastic deformations occur before the limit load according to the stress-strain behavior curve of sand (Figure 7). Therefore, it is necessary to consider plastic deformation in the allowable load and displacement. If allowable displacement is accepted equal to 2.5 cm according to [8], the allowable load according to allowable displacement and safety factors is expressed based on the DSC/HISS and generalized plasticity models in Table 3. The safety factor is computed as ultimate load and allowable load [19].

A comparison of the allowable load for in-situ stress equal to 1.0 and 5.0 kg/cm^2 (Table 3) shows a growth of 48% of the allowable load. It is noted that the bearing capacity for an in-situ stress of 1.0 kg/cm^2 (Figure 14) was equal to Terzaghi's bearing capacity by Equation 15 [19] for Tehran sand and, also, the ultimate load from a finite element analysis was equal to Terzaghi's bearing capacity for Houston sand with an in-situ stress of 100 kPa. Therefore, comparisons between predictions from the models and Terzaghi's equation are valid for an in-situ stress of 1 kg/cm^2 or 100 kPa. The bearing capacity, by Terzaghi's equation, may be expressed for different in-situ stresses corre-

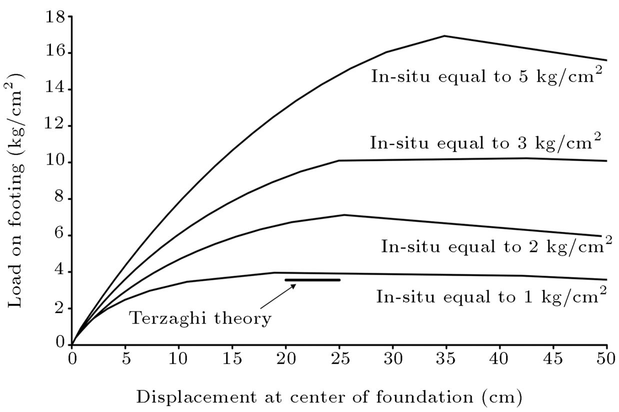

Figure 14. Load-displacement curves for different in-situ stresses for Tehran sand.

Table 3. Allowable load according to 2.5 cm displacement.

In-situ Stress (kg/cm^2)	**Ultimate Load (kg/cm^2)**	**Allowable Load According 2.5 cm Displacement**	**Safety Factor**
1	3.96	1.62 (kg/cm^2)	2.44
2	7.13	1.72 (kg/cm^2)	4.14
3	10.1	1.95 (kg/cm^2)	5.18
5	16.9	2.4 (kg/cm^2)	7.04

sponding to different depths. The obtained ultimate load from such a simulation is greater than the finite element results. Therefore, in-situ stress cannot be assumed equal to equivalent depth. Table 4 shows a comparison between Terzaghi's bearing capacity for different depths, consistent with increasing stress levels and finite element results for Tehran sand.

$$q_{\text{ult}} = cN_c + \gamma D_f N_q + 0.5\gamma B N_\gamma, \tag{15}$$

where q_{ult} is the ultimate bearing capacity, C is the cohesion of soil, N_c, N_q, N_γ are Terzaghi's bearing capacity factors, γ is the effective unit weight of soil, D_f is the distance from ground surface to base of footing and B is the width of square footing.

Table 4 shows that Terzaghi's equation should be modified, with respect to the in-situ stress. Figure 15 shows the bearing capacity from the finite element to the bearing capacity of the Terzaghi theory [19] ratio for both Tehran and Houston sands with friction angles of 31° [18] and 38° [20], respectively, versus in-situ stress (p) to atmospheric pressure (p_a) ratios.

In accordance with Figure 15, the following formula is suggested to determine the bearing capacity, based on in-situ stress for sand:

$$q_u = 0.5 * \gamma * B * N_\gamma^{\text{new}}, \tag{16a}$$

$$N_\gamma^{\text{new}} = N_\gamma * \left(\frac{p}{p_a * \tan(\varphi)}\right)^{\left(\frac{p}{p_a} * n\right)}, \tag{16b}$$

Table 4. Comparison between Terzaghi's bearing capacity for different stress level and the finite element results.

In-Situ Stress	Terzaghi's Bearing Capacity	Finite Element Results
1	3.63	3.96
2	23.63	7.13
3	43.63	10.1
5	83.63	16.9

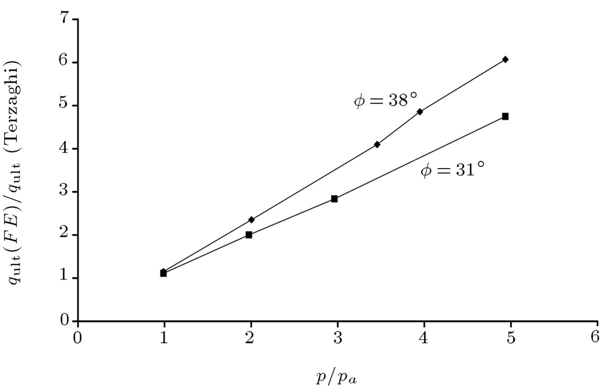

Figure 15. Variation of bearing capacity versus in-situ stress.

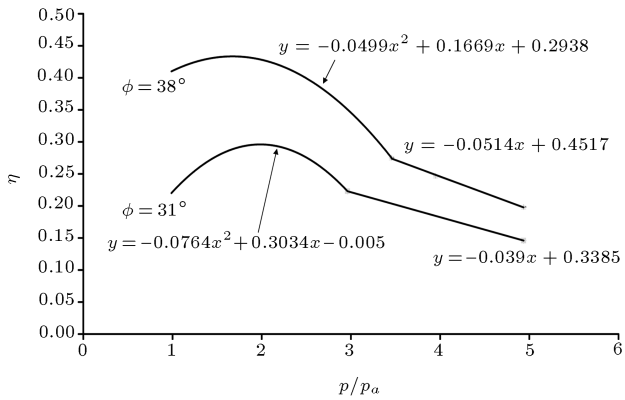

Figure 16. Variation of n versus in-situ stress.

where, N_γ is the same as that expressed by Terzaghi [19], φ is the friction angle obtained from a triaxial test in a laboratory, p is the in-situ stress, p_a is the atmospheric pressure, B is the width of footing, γ is the unit weight of soil and n is determined from Figure 16.

It can be used to interpolate the value of n for different friction angles. Therefore, the bearing capacity of footings on sand can be obtained by Equation 16. This relation is interesting for practicing engineers.

CONCLUSION

A nonlinear finite element method with an eight-noded isoparametric quadrilateral element is used for the prediction of load-deformation behavior, including the bearing capacity of footings. A disturbed state concept, with the HISS plasticity model with associated flow rule, and a generalized plasticity model with non-associated flow rule, is used to characterize the constitutive behavior of soils. Both models are able to simulate load-deformation, including softening behavior, and they both give comparable results for the footing problems. The Drucker-Prager model predicts small deformation prior to ultimate load. This is because the initial elastic zone of the model is larger, in compressive $I_1 - \sqrt{J_2}$ space, than that of other models. Comparisons of load-deformation curves between critical state, Drucker-Prager, modified cap, generalized plasticity and DSC/HISS models show that both GPM and DSC/HISS models give better results than others. In accordance with the obtained results of finite element analyses, the Terzaghi theory was developed for the bearing capacity based on different in-situ stresses. Therefore, engineers will be able to determine the bearing capacity for sand as affected by in-situ stress.

REFERENCES

1. Davidson, H.L. and Chen, W.F. "Nonlinear response of undrained clay to footings", *Computers & Structures*, **7**, pp. 539-546 (1977).

2. Davidson, H.L. and Chen, W.F. "Nonlinear response of drained clay to footings", *Computers & Structures*, **8**, pp. 281-290 (1978).

3. Desai, C.S., Phan, H.V. and Sture, S. "Procedure, selection and application of plasticity models for soil", *Int. J. Numer. Anal. Meth, Geomech.*, **5**, pp. 295-311 (1981).

4. Manoharan, N. and Dasgupta, S.P. "Bearing capacity of surface footings by finite elements", *Computers & Structures*, **54**(4), pp. 563-586 (1995).

5. Manoharan, N. and Dasgupta, S.P. "Collapse load computation for high-friction soil", *Computers & Structures*, **62**(4), pp. 681-684 (1997).

6. Faruque, M.O. and Desai, C.S. "Implementation of a general constitutive model for geological materials", *Int. J. Numer. Anal. Meth. Geomech.*, **9**, pp. 415-436 (1985).

7. Altaee, A., Evgin, E. and Fellenius, B.H. "Finite element validation of a bounding surface plasticity model", *Computers & Structures*, **42**(5), pp. 825-832 (1992).

8. Lee, J. and Salgado, R. "Estimation of bearing capacity of circular footings on sands, based on cone penetration test", *Journal of Geotechnical and Geoenvironmental Engineering*, **131**(4), pp. 442-452 (2005).

9. Akhaveissy, A.H. "Evaluation of tunnel-structure interaction due to strong ground movement", Ph.D. Thesis, Civil Engineering Department, Tarbiat Modares University, Tehran, Iran (in press).

10. Zienkiewicz, O.C., Leung, K.H. and Pastor, M. "Simple model for transient soil loading in earthquake analysis. I. Basic model and its application", *International Journal for Numerical and Analytical Method in Geomechanics*, **9**, pp. 453-476 (1985).

11. Pastor, M., Zienkiewicz, O.C. and Leung, K.H. "Simple model for transient soil loading in earthquake analysis. II. Non-associative models for sand", *International Journal for Numerical and Analytical Method in Geomechanics*, **9**, pp. 477-498 (1985).

12. Chen, W.F. and Baladi, G.Y. "Soil plasticity theory and implementation", *Developments in Geotechnical Engineering*, **38**, Elsevier Science Publishers, New York, USA (1985).

13. Pastor, M., Zienkiewicz, O.C. and Chan, A.H.C. "Generalized plasticity and the modelling of soil behaviour", *International Journal for Numerical and Analytical Method in Geomechanics*, **14**, pp. 151-190, (1990).

14. Liu, H. and Ling, H.I. "A sand model based on generalized plasticity", *15th ASCE Engineering Mechanics Conference*, USA, Columbia University, New York, USA (2002).

15. Liu, H. and Song, E. "Seismic response of large underground structures in liquefiable soils subjected to horizontal and vertical earthquake excitations", *Computers and Geotechnics*, **32**, pp. 223-244 (2005).

16. Desai, C.S., *Mechanics of Materials and Interfaces: The Disturbed State Concept*, CRC Press, Boca Raton, Florida, USA (2001).

17. Roscoe, K.H., Schofield, A.N. and Wroth, C.P. "On the yielding of soils", *Geotechnique*, **8**(1), pp. 22-52 (1968).

18. Report of PEY JOU IRAN Consulting Engineers, "Triaxial test for Azadi Square", Library of Tehran Urban Subway Company.

19. Liu, C. and Evett, J.B., *Soils and Foundations*, pp. 123-166, Prentice-Hall, Inc., Englewood Cliffs, NJ, USA (1981).

20. Nesnas, K. and Woodward, P. "Advanced bearing capacity computation of a footing on sand using a kinematic hardening elastoplastic model", *Numerical Model in Geomechanics- NUMOG VII*, Pande, Pietruszczak & Schweiger, Eds., Balkema, Rotterdam, pp. 463-468 (1999).